Optical and luminescence properties of Nd^{3+} ions in K–Ba–Al-phosphate and fluorophosphate glasses

2006 J. Phys.: Condens. Matter 18 165

(http://iopscience.iop.org/0953-8984/18/1/012)

INSTITUTE OF PHYSICS PUBLISHING JOURNAL OF PHYSICS: CONDENSED MATTER

J. Phys.: Condens. Matter **18** (2006) 165–179 doi:10.1088/0953-8984/18/1/012

Optical and luminescence properties of Nd^{3+} ions in K–Ba–Al-phosphate and fluorophosphate glasses

R Balakrishnaiah[1], P Babu[1], C K Jayasankar[1,4], A S Joshi[2], A Speghini[3] and M Bettinelli[3]

[1] Department of Physics, Sri Venkateswara University, Tirupati-517 502, India
[2] High Power Laser Optics Laboratory, Laser Plasma Division, Centre for Advanced Technology, Indore-452 013, India
[3] Dipartimento Scientifico e Tecnologico, Università di Verona and INSTM, UdR Verona, Ca'Vignal, Strada Le Grazie 15, I-37134 Verona, Italy

E-mail: ckjaya@yahoo.com

Received 8 August 2005, in final form 9 November 2005
Published 9 December 2005
Online at stacks.iop.org/JPhysCM/18/165

Abstract

Phosphate (PKBAN: $P_2O_5+K_2O+BaO+Al_2O_3+Nd_2O_3$) and fluorophosphate (PKBFAN: $P_2O_5 + K_2O + BaO + BaF_2 + Al_2O_3 + Nd_2O_3$ and PKBAFN: $P_2O_5 + K_2O + BaO + Al_2O_3 + AlF_3 + Nd_2O_3$) glasses were prepared with three concentrations (0.1, 1.0 and 2.0 mol%) of Nd^{3+} ions and their detailed luminescence properties have been investigated. Absorption spectra for 1.0 mol% of Nd^{3+}-doped glasses have been analysed using Judd–Ofelt (JO) theory. The observed bands in absorption spectra from ground to excited states are assigned and analysed with the parameterized free-ion Hamiltonian model. The JO parameters have been used to predict radiative properties for $^4F_{3/2} \rightarrow {}^4I_J$ ($J = 15/2, 13/2, 11/2$ and $9/2$) transitions of Nd^{3+} ions in these glasses. The Inokuti–Hirayama model has been applied to the non-exponential behaviour of the decay profiles to investigate the mechanism involved in the energy transfer between the donors and acceptors.

1. Introduction

Glasses doped with lanthanide ions (Ln^{3+}) are very promising and attractive for developing and tailoring optical devices such as lasers, optical fibres, acousto-optic modifiers and planar waveguides. Among various glass hosts, phosphate glasses have received much attention because they can store optical energy at greater densities than other hosts and this energy can be efficiently extracted. Further, phosphate glasses exhibit low refractive index, low dispersion and very good thermo-optical qualities. Also, they can be easily prepared in various

[4] Author to whom any correspondence should be addressed.

Table 1. Glass compositions and glass labels of the Nd^{3+}-doped glasses.

Glass composition	Glass labels
58.95 P_2O_5 + 17.45 K_2O + 14.5 BaO + 9 Al_2O_3 + 0.1 Nd_2O_3	PKBAN(1)
58.5 P_2O_5 + 17 K_2O + 14.5 BaO + 9 Al_2O_3 + 1 Nd_2O_3	PKBAN(2)
58 P_2O_5 + 17 K_2O + 14 BaO + 9 Al_2O_3 + 2 Nd_2O_3	PKBAN(3)
55.95 P_2O_5 + 17 K_2O + 11.95 BaO + 6 BaF_2 + 9 Al_2O_3 + 0.1 Nd_2O_3	PKBFAN(1)
55.5 P_2O_5 + 17 K_2O + 11.5 BaO + 6 BaF_2 + 9 Al_2O_3 + 1 Nd_2O_3	PKBFAN(2)
55 P_2O_5 + 17 K_2O + 11 BaO + 6 BaF_2 + 9 Al_2O_3 + 2 Nd_2O_3	PKBFAN(3)
56.6 P_2O_5 + 16.75 K_2O + 14.73 BaO + 8.37 Al_2O_3 + 3.45 AlF_3 + 0.1 Nd_2O_3	PKBAFN(1)
56.15 P_2O_5 + 16.75 K_2O + 14.28 BaO + 8.37 Al_2O_3 + 3.45 AlF_3 + 1 Nd_2O_3	PKBAFN(2)
55.65 P_2O_5 + 16.75 K_2O + 13.78 BaO + 8.37 Al_2O_3 + 3.45 AlF_3 + 2 Nd_2O_3	PKBAFN(3)

compositions and can preserve their useful properties when doped with significant amounts of active Ln^{3+} ions.

Among the phosphate glasses, alkali and alkaline-earth metaphosphate glasses are very attractive hosts due to their high transparency nature to ultraviolet light. The only disadvantage in these glasses is their hygroscopic nature, but the selection of $Al(PO_3)_3$, $Ba(PO_3)_2$, $Mg(PO_3)_2$ and KH_2PO_4 as starting materials for phosphate composition has its own advantages compared to other metaphosphates [1]. Here, $Al(PO_3)_3$ is added to improve the physical properties of glass. Further, addition of fluoride content increases the resistance to water and hence decreases the non-radiative relaxation of the emitting level.

Among the trivalent Ln^{3+} ions, Nd^{3+} is one of the most extensively studied ions for solid-state lasers due to its laser emission at a very useful wavelength, 1064 nm, in addition to the possibility of lasing at other wavelengths such as 1800, 1350 and 880 nm at room temperature. Also, its absorption in the UV–VIS–NIR regions allows efficient pumping either with broad-band sources (xenon lamp) or with sources of selected wavelength using diode lasers [1, 2].

Since the first demonstration of laser action in neodymium-doped glass by Snitzer [3], considerable progress has been made in evaluating the effects of these amorphous host materials on the Nd^{3+} laser ion. Nd^{3+}-doped phosphate glasses are found to be very attractive gain media for high energy and high peak power lasers which can be prepared even in bulk sizes with high optical homogeneity and purity. Among various phosphate glass compositions, the P_2O_5 + K_2O + MO + Al_2O_3, (MO = BaO, MgO, SrO, CaO) composition is found to be an excellent host for laser media. However, for this composition, a detailed and systematic optical and luminescence study, including compositional and concentration variations, has not been available in the literature to the best of our knowledge. The aim of the present study is to examine various lasing parameters (lifetime, peak stimulated emission cross section, quantum efficiency, etc) among various phosphate glass hosts to establish the relation between the spectroscopic properties of different concentrations of Nd^{3+} ions and compositional variations in glass host. Hence, the present work reports the detailed and systematic spectroscopic studies of phosphate (PKBAN(M)) and fluorophosphate (PKBFAN(M) and PKBAFN(M)) glasses for different concentrations of Nd^{3+} ions, where M = 1, 2 and 3 refers to 0.1, 1.0 and 2.0 mol% Nd^{3+} ion concentrations, respectively (see table 1).

2. Experimental details

The glasses in the present investigation were prepared by a conventional melt-quenching technique at ambient atmosphere. The chemical compositions (in mol%) and labels of the glasses are presented in table 1.

Table 2. Physical properties of 1.0 mol% Nd^{3+}-doped glasses.

Properties	PKBAN(2)	PKBFAN(2)	PKBAFN(2)
Refractive index, n	1.525	1.532	1.541
Density, d (g cm^{-3})	2.67	2.93	2.83
Concentration, C (10^{20} ions cm^{-3})	2.30	2.49	2.43
Optical path length (cm)	0.420	0.359	0.358

High-purity chemicals of $Al(PO_3)_3$, $Ba(PO_3)_2$, KH_2PO_4, BaF_2, AlF_3 and Nd_2O_3 were used as starting materials. After being well ground in a mortar with a pestle, the mixed reagents were put into a platinum crucible and kept in an electric furnace around 1050–1100 °C for 1 h and then poured onto a preheated brass plate. Then the formed glasses were annealed at 350 °C for ten hours to remove thermal strains. Finally, the glass samples were polished with silicon carbide abrasive paper and finally with an FIS polishing film to achieve a very smooth surface.

The densities of the samples were determined by Archimedes' method with water as the immersion liquid. The refractive indices were measured on an Abbe refractometer at sodium wavelength (589.3 nm) with 1-bromonapthalene as the contact liquid. Table 2 presents the physical properties for 1.0 mol% Nd^{3+}-doped glasses. Absorption spectra (300–1000 nm) were recorded using a Hitachi U-3400 spectrophotometer. The NIR emission spectra (800–1600 nm) were recorded using a Jarrell-Ash 3/4 m Czerny–Turner single monochromator. The signal was detected by a liquid nitrogen-cooled Northcoast EO-817P germanium detector connected to a computer-controlled Stanford Research SR510 lock-in amplifier. The emission decay curves were measured by exciting the samples with a pulsed Nd-YAG laser ($\lambda_{exc} = 355$ nm). The signal was then analysed using a 0.5 m monochromator equipped with a 150 lines mm^{-1} grating and detected with a GaAs PMT and a digital oscilloscope.

3. Theory

3.1. Energy level analysis, free-ion and bonding parameters

A model Hamiltonian expressed in terms of free-ion or atomic parameters is used to analyse the free-ion energy levels involved in f–f transitions. The H_{FI} that represents the energy level structure of Nd^{3+} ($4f^3$) ion is defined and used in the calculation as [4–8]

$$\hat{H}_{FI} = E_{AVG} + \sum_k F^k \hat{f}_k + \xi_{SO}\hat{A}_{SO} + \alpha\hat{L}(\hat{L}+1) + \beta\hat{G}(G_2) + \gamma\hat{G}(R_7) + \sum_i T^i \hat{t}_i + \sum_k P^k \hat{p}_k + \sum_j M^j \hat{m}_j, \quad (1)$$

where $k = 2$, 4 and 6; $i = 2$, 3, 4, 6, 7 and 8; and $j = 0$, 2 and 4. The operators ($\hat{f}$, $\hat{A}_{SO}$, $\hat{L}$, $\hat{G}$, $\hat{t}_i$, $\hat{p}_k$ and $\hat{m}_j$) and their associated parameters (central field, E_{AVG}; two-body electrostatic repulsion, F^2, F^4 and F^6; spin–orbit, ξ; two-body configuration, α, β and γ; three-body configuration, T^2, T^3, T^4, T^6, T^7 and T^8; spin–other-orbit, M^0, M^2 and M^4 and electrostatically correlated spin–orbit, P^2, P^4 and P^6) are written according to conventional notation and meaning [4–8]. The operators represent angular integrals and their associated parameters represent radial integrals, where the former can be evaluated exactly and the latter can be determined by a semi-empirical approach [4].

The fitting procedure between experimental and calculated energy level values involves the standard least-square fit method to get the free-ion parameters given in equation (1) along with the minimum values of rms deviation (σ) as a figure of merit in describing the quality of

the fit. σ is defined as [6]

$$\sigma = \left(\frac{\sum (E_i^{\exp} - E_i^{\text{cal}})^2}{N} \right)^{\frac{1}{2}}, \tag{2}$$

where $E_i^{\exp}$ and E_i^{cal} are the experimentally observed and calculated energies for level i, and N denotes the total number of levels included in the energy level fit.

The nephelauxetic ratio β and the bonding parameter δ are defined as [6, 9]

$$\beta = \bar{\nu}_c/\bar{\nu}_f \qquad \text{and} \qquad \delta = [(1 - \bar{\beta})/\bar{\beta}] \times 100, \tag{3}$$

where $\bar{\nu}_c$ and $\bar{\nu}_f$ refer to the wavenumbers of the corresponding transitions in the complex and free ion, respectively. The β values for all the observed transitions are computed and their average value ($\bar{\beta}$) is used to estimate the bonding parameter δ (in per cent) for each system. Depending on the ligands, the value of δ may be positive or negative, indicating covalent or ionic bonding, respectively [6, 9].

3.2. Absorption spectra and Judd–Ofelt analysis

The optical absorption spectra of Ln^{3+} ions serve as a basis for understanding their spectroscopic properties [10–15]. Intensities of the absorption bands are usually expressed in terms of oscillator strengths (f) which are statistically weighted to account for the degeneracy of the initial state and are calculated by using the following formula [15].

$$f_{\exp} = 4.32 \times 10^{-9} \int \varepsilon(\upsilon)\, \mathrm{d}\upsilon, \tag{4}$$

where ε is the molar absorptivity at energy ν cm^{-1}.

The Judd–Ofelt model [16, 17] gives the theoretical estimation of the intensities of intra-configurational f–f transitions of Ln^{3+} ions. According to this model, the transition intensities are characterized by three phenomenological parameters known as JO intensity parameters, Ω_λ ($\lambda = 2, 4$ and 6), which depend on the local environment. Although a few magnetic dipole transitions exist, the majority of these transitions are induced electric–dipole transitions. The oscillator strength of an electric–dipole transition $\Psi J \rightarrow \Psi' J'$ is given by

$$f_{\text{cal}} = \frac{8\pi^2 mc\upsilon}{3h(2J+1)} \frac{(n^2+2)^2}{9n} \sum_{\lambda=2,4,6} \Omega_\lambda (\Psi J \| U^\lambda \| \Psi' J')^2, \tag{5}$$

where h is Planck's constant, n is the refractive index of the medium, c is the velocity of light in vacuum, m is the rest mass of an electron, υ is the mean energy of the transition in cm^{-1}, J is the total angular momentum quantum number of the initial state and $\|U^\lambda\|$ are the doubly reduced matrix elements of the unit tensor operator of rank $\lambda = 2, 4$ and 6 which are calculated using intermediate coupling approximation [15] for the transition $\Psi J \rightarrow \Psi' J'$.

The experimental oscillator strengths ($f_{\exp}$) for various transitions are evaluated using equation (4) and are used in equation (5). A least-square fitting approximation is then used to determine the Ω_λ parameters which give the best fit between experimental and calculated oscillator strengths. The relative magnitudes of the Ω_λ parameters are useful for explaining the bonding, symmetry and stiffness of the host matrices [2].

3.3. Radiative properties

The JO parameters are used to predict radiative properties. Although only a few magnetic dipole transitions exist for the trivalent Ln^{3+} ions, these transitions are of interest, because

their intensities are in a first-order approximation, independent of the ligand environment and can thus be used as intensity standards. Moreover, the intensity of a magnetic dipole transition can be calculated provided that suitable wavefunctions are available.

The electric (S_{ed}) and the magnetic (S_{md}) dipole line strengths of a transition $\Psi J \rightarrow \Psi' J'$ are given by [15]

$$S_{ed} = e^2 \sum_{\lambda=2,4,6} \Omega_\lambda (\Psi J \| U^\lambda \| \Psi' J')^2 \tag{6}$$

and

$$S_{md} = \frac{e^2 h^2}{16\pi^2 m^2 c^2} \left(\Psi J \| L + 2S \| \Psi' J'\right)^2, \tag{7}$$

respectively. The radiative transition probability (A) for the transition $\Psi J \rightarrow \Psi' J'$ can be evaluated from the relation

$$A\left(\Psi J, \Psi' J'\right) = \frac{64\pi^4}{3h(2J+1)\lambda^3} \left(\frac{n(n^2+2)^2}{9} S_{ed} + n^3 S_{md}\right) \tag{8}$$

and the fluorescence branching ratio (β_R) can be obtained from the expression

$$\beta_R\left(\Psi J, \Psi' J'\right) = \frac{A\left(\Psi J, \Psi' J'\right)}{A_T} \tag{9}$$

where A_T is the total radiative transition probability of ΨJ state, given by

$$A_T\left(\Psi J\right) = \sum A\left(\Psi J, \Psi' J'\right). \tag{10}$$

The radiative lifetime (τ_R) of ΨJ level is given by

$$\tau_R(\Psi J) = (A_T(\Psi J))^{-1} = \left(\sum A(\Psi J, \Psi' J')\right)^{-1}. \tag{11}$$

The peak stimulated emission cross-section ($\sigma(\lambda_p)$) for the transition $\Psi J \rightarrow \Psi' J'$ is given by

$$\sigma(\lambda_p)(\Psi J, \Psi' J') = \frac{\lambda_p^4}{8\pi c n^2 \Delta\lambda_{eff}} A(\Psi J, \Psi' J'), \tag{12}$$

where λ_p is the emission peak wavelength and $\Delta\lambda_{eff}$ is the effective bandwidth of the transition $\Psi J \rightarrow \Psi' J'$.

3.4. Fluorescence decay: energy transfer

An excited Ln^{3+} (here, Nd^{3+}) ion may relax to the initial ground state through radiative transition or phonon emission or by transferring its excess energy to a nearby Ln^{3+} ion or by a combination of relaxations [18–20]. In general, at low concentrations of dopant ions, the interaction between optically active Ln^{3+} ions is negligible and the fluorescence decay curves can be fitted straight away to a single exponential function to determine the lifetime of the emitting level. However, when the concentration is large enough, the interaction between these ions becomes so prominent that energy transfer takes place from an excited Ln^{3+} ion (donor) to a non-excited Ln^{3+} (acceptor) ion, leading to a non-exponential shape of the decay curves. But in the case of Nd^{3+} ion, even for low Nd^{3+} ion concentrations (0.1 mol%), the behaviour is not perfectly single exponential. The non-exponential decay curves may be fitted to a bi-exponential function and the average lifetime can be evaluated [18, 19].

The non-exponential nature of the fluorescence decay curves can be analysed by fitting the data in the framework of the Inokuti–Hirayama (IH) model [20] to disclose the dominant

mechanism of interaction. According to this model, the decay of the fluorescence intensity follows the equation

$$I(t) = I_0 \exp\left(-\left(\frac{t}{\tau_0}\right) - Q\left(\frac{t}{\tau_0}\right)^{3/S}\right), \tag{13}$$

where t is the time after pulsed excitation and τ_0 is the intrinsic decay time of the donors in the absence of acceptors. The value $S = 6, 8$ or 10 depends on whether the dominant mechanism of interaction is dipole–dipole, dipole–quadrupole or quadrupole–quadrupole, respectively. The energy-transfer parameter Q is defined as

$$Q = \frac{4\pi}{3}\Gamma\left(1 - \frac{3}{S}\right) N_0 R_0^3, \tag{14}$$

where the Γ function, $\Gamma(x)$, is equal to 1.77 in the case of dipole–dipole interaction ($S = 6$), 1.43 for dipole–quadrupole interactions ($S = 8$) and 1.3 for quadrupole–quadrupole interactions ($S = 10$). N_0 is the concentration of acceptors, which is in practice equal to the concentration of Ln^{3+} ions, and R_0 is the critical distance defined as the donor–acceptor separation for which the rate of energy transfer to the acceptors is equal to the rate of intrinsic decay of the donors. The parameter Q can be derived in the fitting process of decay data. The τ_0 used in equation (13) corresponds to the case of isolated donors, where no energy transfer takes place and the exponential decay curves exhibit perfect single exponential nature. The donor–acceptor energy-transfer parameter C_{DA} is related to R_0 by the formula

$$C_{DA} = R_0^S \tau_0^{-1}. \tag{15}$$

4. Results

4.1. Energy level analysis, free-ion and bonding parameters

The room-temperature optical absorption spectra of 1.0 mol% Nd^{3+}-doped PKBAN(2), PKBFAN(2) and PKBAFN(2) glasses are shown in figure 1. Table 3 shows the observed (E_{exp}) and calculated (E_{cal}) free-ion energy positions and their empirical free-ion parameters for the present systems along with some other reported Nd^{3+}: systems that include BaLiBO ($BaCO_3 + LiCO_3 + H_3BO_3$) glasses [5], $NdAlO_3$ [6, 21], PSP (potassium sodium phosphate) glasses [22] and free ion [23]. The hydrogenic ratios F^2/F^4 and F^2/F^6, the net electrostatic field $\sum F^k$, the average nephelauxetic ratio ($\bar{\beta}$) and the bonding parameter (δ) are also shown in table 3.

4.2. Optical absorption spectra—Judd–Ofelt parameters and radiative properties

From the optical absorption spectra (figure 1) the experimental oscillator strengths are estimated using equation (4) and the best-fit JO parameters are determined using equation (5) as carried out for other Nd^{3+}:glasses [10–14, 24–27]. Though the contribution due to the magnetic dipole is negligible, we determined those values also [5, 7]. The experimental and calculated oscillator strengths for the present glasses along with experimental oscillator strengths for Nd^{3+}:phosphate glass ($57P_2O_5 + 28.5BaO + 14.5K_2O$ (BKP)) reported by Ajroud *et al* [2] and Nd^{3+}:fluoroborophosphate glass (Glass C:$78NaH_2PO_4{\cdot}H_2O + 10H_3BO_3 + 10BaF_2 + 2NdF_3$ (FBP)) reported by Kumar *et al* [24] are shown in table 4 for comparison. The JO parameters, spectroscopic quality parameter, radiative and fluorescence lifetimes and quantum efficiencies for the title glasses along with the reported glasses [2, 24] as well as commercial LG-750 glass [1, 28] are shown in table 5. The JO parameters have been used to predict radiative properties such as transition probabilities (A), radiative lifetimes (τ_{rad}) and branching ratios (β_R) for the luminescent $^4F_{3/2}$ level of Nd^{3+} ion in the present hosts (using equations (8)–(11)).

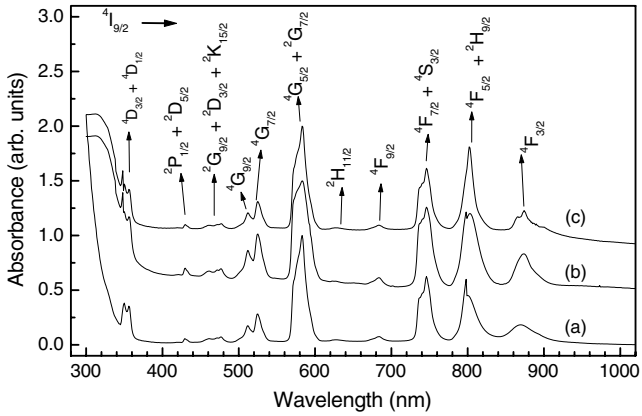

Figure 1. Optical absorption spectra of Nd^{3+} ions in (a) PKBAN(2), (b) PKBFAN(2) and (c) PKBAFN(2) glasses.

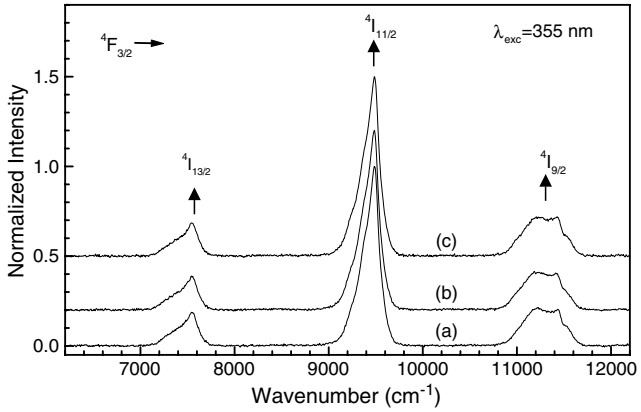

Figure 2. Emission spectra of Nd^{3+} ions in (a) PKBAN(2), (b) PKBFAN(2) and (c) PKBAFN(2) glasses.

4.3. Luminescence properties

The emission spectra for the $^4F_{3/2} \rightarrow {}^4I_J$ ($J = 13/2, 11/2$ and $9/2$) transitions are shown in figure 2 and the decay profiles of $^4F_{3/2} \rightarrow {}^4I_{13/2}$ for all the title glasses are shown in figure 3. The calculated branching ratios (based on JO parameters) and their experimental values (from the analysis of fluorescence spectra) are shown in table 6. The peak stimulated emission cross-sections ($\sigma(\lambda_p)$) for the transitions $^4F_{3/2} \rightarrow {}^4I_J$ are determined using equation (12) and those for the $^4F_{3/2} \rightarrow {}^4I_{11/2}$ transition are presented in table 6. The non-exponential decay curves obtained for various concentrations have been analysed using the IH model fit and various parameters (N_0, the concentration of acceptor ions; τ_{flu} and τ_0, the experimental and the intrinsic lifetimes, respectively; Q, the energy-transfer fitting parameter; R_0 and R, the critical and mean distances between the donor and acceptor ions, respectively; and C_{DA}, the dipole–dipole interaction parameter) have been evaluated which are presented in table 7.

Table 3. Experimental (E_{exp}) and calculated (E_{cal}) energy levels (cm^{-1}), best-fit free-ion parameters (cm^{-1}), average nephelauxetic ratio ($\bar{\beta}$) and the bonding parameter (δ) along with hydrogenic ratios for Nd^{3+}:complexes.

Transition	PKBAN(2)		PKBFAN(2)		PKBAFN(2)		BaLiBO [5]	$NdAlO_3$ [6, 21]	PSP [22]	Free-ion [23]
$^4I_{9/2} \rightarrow$	E_{exp}	E_{cal}	E_{exp}	E_{cal}	E_{exp}	E_{cal}	E_{exp}	E_{exp}	E_{exp}	E_{exp}
$^4I_{9/2}$	0	25	0	3	0	9	0	0	0	0
$^4I_{11/2}$	1 781	1 845	1 761	1 822	1 795	1 842	—	1 913	—	1 398
$^4I_{13/2}$	3 793	3 725	3 774	3 705	3 739	3 801	—	3 895	—	2 893
$^4I_{15/2}$	—	5 829	—	5 812	—	5 846	—	5 975	—	4 454
$^4F_{3/2}$	11 507	11 399	11 442	11 397	11 442	11 391	—	11 268	11 571	9371
$^4F_{5/2}$	12 453	12 407	12 453	12 411	12 469	12 410	12 442	12 256	—	10 138
$^2H(2)_{9/2}$	12 531	12 677	12 531	12 632	12 531	12 628	12 566	12 459	12 584	10 033
$^4F_{7/2}$	13 405	13 366	13 405	13 372	13 405	13 373	13 383	13 285	13 567	10 859
$^4S_{3/2}$	13 477	13 455	13 514	13 458	13 477	13 459	13 519	13 372	—	10 950
$^4F_{9/2}$	14 620	14 638	14 620	14 630	14 620	14 638	14 734	14 557	14 767	11 762
$^2H_{11/2}$	15 949	15 957	15 949	15 904	15 924	15 915	15 972	15 725	—	12 495
$^4G_{5/2}$	17 153	17 154	17 153	17 173	17 153	17 154	17 138	16 857	17 356	14 187
$^2G_{7/2}$	17 483	17 296	17 422	17 295	17 391	17 284	17 286	17 151	—	13 888
$^4G_{7/2}$	19 048	19 047	19 048	19 051	19 048	19 044	18 979	18 787	19 225	15 443
$^4G_{9/2}$	19 531	19 409	19 531	19 425	19 531	19 420	19 531	—	19 564	15 705
$^2K_{13/2}$	—	19 681	—	19 628	—	19 623	—	—	—	16 089
$^2G_{9/2}$	20 964	21 043	20 921	21 034	20 964	21 041	21 191	20 792	—	16 764
$^2D_{3/2}$	21 322	21 292	21 186	21 205	21 186	21 200	—	20 815	—	17 096
$^4G_{11/2}$	—	21 367	—	21 393	—	21 392	—	—	—	17 410
$^2K_{15/2}$	21 692	21 636	21 645	21 584	21 645	21 586	21 673	—	—	17 642
$^2P_{1/2}$	23 310	23 309	23 256	23 232	23 256	23 228	23 245	22 990	—	18 694
$^2D_{5/2}$	23 866	23 867	23 810	23 827	23 810	23 821	—	23 579	—	19 046
$^2P_{3/2}$	—	26 180	—	26 087	—	26 101	—	25 883	—	20 857
$^4D_{3/2}$	27 933	28 108	28 011	28 147	28 011	28 111	27 988	27 654	—	23 092
$^4D_{5/2}$	—	28279	—	28300	—	28265	—	—	—	23 246
$^4D_{1/2}$	28 571	28 600	28 653	28 645	28 571	28 615	28 588	28 264	—	23 465
$^2H(1)_{9/2}$	—	32 912	—	32 803	—	32 794	—	32 523	—	—
$\sigma(N)$	±81 (21)		±66 (21)		±58 (21)		±34 (16)	±52 (22)	±67 (8)	±79 (26)
Parameters										
$\bar{\beta}$	1.230		1.228		1.240		1.251	1.241	1.255	—
δ	−18.699		−18.567		−19.355		−20.064	−19.400	−20.319	—
E_{AVG}	24 244		24 199		24 193		24 233	23 929	23 479	19 581
F^2	72 729		72 480		72 402		72 285	71 436	64 082	58 973
F^4	53 450		53 615		53 462		52 594	51 905	63 128	43 023
F^6	36 282		35 568		35 616		35 750	35 242	22 636	27 018
ξ	863		864		867		900	880	866	660
$\sum F^k$	162 461		161 663		161 480		160 629	158 583	149 846	129 014
F^2/F^4	1.361		1.352		1.354		1.374	1.376	1.015	1.371
F^2/F^6	2.005		2.038		2.033		2.022	2.027	2.831	2.183

5. Discussion

5.1. Absorption spectra: energy level analysis

The optical absorption spectra for the title glass samples were recorded at room temperature. The transitions in the absorption spectrum were assigned with the help of earlier work [1, 2, 5, 7, 10–14] as they do not differ much from each other. These spectra are

Table 4. Experimental (f_{exp}) and calculated (f_{cal}) oscillator strengths (10^{-6} units) for the Nd^{3+}:glasses.

Transition	PKBAN(2)		PKBFAN(2)		PKBAFN(2)		FBP [24]	BKP [2]
$^4I_{9/2} \rightarrow$	f_{exp}	f_{cal}	f_{exp}	f_{cal}	f_{exp}	f_{cal}	f_{exp}	f_{exp}
$^4F_{3/2}$	3.96	3.57	3.85	3.96	2.69	3.20	2.57	1.82
$^4F_{5/2}$, $^2H_{9/2}$	10.98	11.61	10.93	11.12	10.44	10.03	7.74	6.76
$^4F_{7/2}$, $^4S_{3/2}$	12.44	12.10	10.85	10.86	9.82	10.28	8.06	6.63
$^4F_{9/2}$	0.95	0.94	0.74	0.86	0.68	0.80	2.67	0.75
$^2H_{11/2}$	0.19	0.26	0.09	0.24	0.38	0.22	4.05	—
$^4G_{5/2}$, $^2G_{7/2}$	35.17	35.20	25.17	25.24	27.61	27.67	17.75	15.68
$^4G_{7/2}$	6.26	5.87	6.59	5.58	5.68	5.02	5.46	4.30
$^4G_{9/2}$	4.97	3.34	5.21	3.29	4.65	2.88	6.18	
$^2G_{9/2}$, $^2D_{3/2}$, $^2K_{15/2}$	2.52	2.05	2.39	2.10	2.23	1.80	4.21	4.57
$^2P_{1/2}$, $^2D_{5/2}$	0.92	1.02	1.09	1.20	0.85	0.93	—	2.00
$^4D_{3/2}$, $^4D_{1/2}$	16.27	16.54	18.84	19.21	14.77	15.10	—	10.02
$\sigma(N)$	±0.59 (11)		±0.68 (11)		±0.64 (11)		±0.20 (9)	±2.20 (9)

Table 5. Judd–Ofelt parameters (Ω_λ), lifetimes τ ($^4F_{3/2}$), quality parameter (X) and quantum efficiency (η) for 1.0 mol% Nd^{3+}:glasses.

Glass	PKBAN(2)	PKBFAN(2)	PKBAFN(2)	BKP [2]	FBP [24]	LG-750 [1, 28]
Ω_2 (10^{-20} cm^2)	9.23	4.49	6.60	3.28	2.90	4.6
Ω_4 (10^{-20} cm^2)	7.00	8.28	6.36	3.54	5.20	4.8
Ω_6 (10^{-20} cm^2)	8.74	7.66	7.30	4.67	7.30	5.6
$X = \Omega_4/\Omega_6$	0.80	1.08	0.87	0.76	0.71	0.86
τ_{rad} ($^4F_{3/2}$) (μs)	214	211	244	430	271	367
τ_{flu} ($^4F_{3/2}$) (μs)	144	189	169	190	160	—
$\eta = \tau_{flu}/\tau_{rad}$	0.67	0.90	0.69	0.44	0.59	—

Table 6. Emission characteristics of $^4F_{3/2} \rightarrow {}^4I_J$ transitions in Nd^{3+}:glasses.

	β_R $^4F_{3/2} \rightarrow$										
	$^4I_{15/2}$		$^4I_{13/2}$		$^4I_{11/2}$		$^4I_{9/2}$		λ_p	$\sigma(\lambda_p)$	$\Delta\lambda_{eff}$
Glass	Exp	Cal	Exp	Cal	Exp	Cal	Exp	Cal	($^4F_{3/2} \rightarrow {}^4I_{11/2}$) (nm)	($^4F_{3/2} \rightarrow {}^4I_{11/2}$) ($10^{-20}$ cm^2)	($^4F_{3/2} \rightarrow {}^4I_{11/2}$) (nm)
PKBAN(2)	—	0.01	0.13	0.10	0.59	0.50	0.28	0.39	1054.4	6.48	25.5
PKBFAN(2)	—	0.01	0.13	0.09	0.59	0.47	0.28	0.43	1054.4	6.23	25.1
PKBAFN(2)	—	0.01	0.13	0.10	0.59	0.49	0.28	0.40	1054.4	5.27	26.5
BKP [2]	—	—	0.11	—	0.53	—	0.35	—	1059	2.78	29.3
FBP [24]	—	—	0.09	—	0.55	—	0.35	—	1057	4.70	27.5
LG-750 [1, 28]	—	—	—	—	—	—	—	—	1053.5	3.70	25.3

characterized by absorption bands associated with transitions from the ground $^4I_{9/2}$ level of Nd^{3+} ion to $^4F_{3/2,5/2,7/2,9/2}$, $^2H_{9/2,11/2}$, $^4S_{3/2}$, $^4G_{5/2,7/2,9/2}$, $^2G_{7/2,9/2}$, $^2K_{15/2}$, $^2P_{1/2}$, $^4D_{3/2}$ and $^4D_{1/2}$ excited levels. The band positions and intensities closely resemble the absorption spectra of Nd^{3+} ions in glass media [1, 2, 5, 7, 10–14], though there is a slight variation in the relative locations and intensities of the bands due to change in the glass composition.

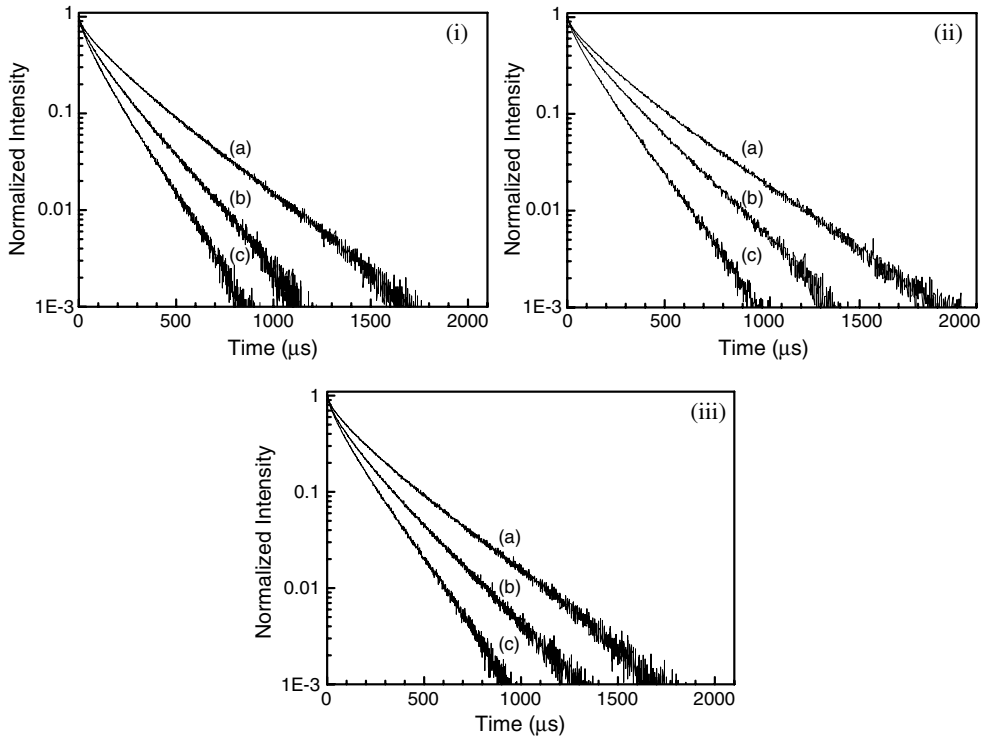

Figure 3. Luminescence decay profiles for the $^4F_{3/2} \rightarrow {}^4I_{13/2}$ state of the Nd^{3+} ion in (i) PKBAN, (ii) PKBFAN and (iii) PKBAFN glasses for (a) 0.1 mol%, (b) 1.0 mol% and (c) 2.0 mol% Nd^{3+} ion concentrations.

Table 7. Various spectroscopic parameter (N_0, τ_{flu}, τ_0, Q, R_0, C_{DA}, W_{n-r} and A_r) values obtained from decay curve analysis for Nd^{3+}:glasses along with reported systems. (See table 1 for glass labels and text for the details of parameter meanings.)

Glass	N_0 (10^{20} ions cm^{-3})	τ_{flu} (μs)	τ_0 (μs)	Q	R_0 (nm)	R (nm)	C_{DA} (10^{-40} cm^6 s^{-1})	W_{n-r} (s^{-1})	A_r (s^{-1})
PKBAN(1)	0.246	232							
PKBAN(2)	2.300	144	232	0.86	0.80	1.01	10.97	2272	4674
PKBAN(3)	4.904	121		1.33	0.72	0.79	5.76	3592	
PKBFAN(1)	0.248	256							
PKBFAN(2)	2.489	189	256	0.67	0.71	0.99	5.06	552	4750
PKBFAN(3)	4.935	132		1.24	0.70	0.79	4.49	2836	
PKBAFN(1)	0.247	234							
PKBAFN(2)	2.427	169	234	0.75	0.75	0.99	7.35	1819	4099
PKBAFN(3)	4.782	131		1.15	0.69	0.79	4.45	3535	
Nd:YAG [36]	1.2 at.%	—	170	—	0.56	—	1.8	—	—
Nd^{3+}:$YAlO_3$ [37]	0.1 at.%	—	175	—	0.52	—	1.5	—	—

5.2. Free-ion and bonding parameters

The experimental energy level positions for all the transitions from the ground $^4I_{9/2}$ state to various excited states of Nd^{3+} ion in the titled hosts are measured from the absorption (figure 1) as well as emission spectra (figure 2) and are presented in table 3. In table 3, the blank spaces

under the E_{exp} columns indicate that these transitions are not observed, which may be due to the fact that they are very weak, overlapped by stronger bands or forbidden by selection rules. The observed energy levels have been analysed using H_{FI} as defined in equation (1). In the present systematic energy level fitting, only F^k and ξ were varied for all the systems using the initial parameter values of Nd^{3+}:$LaCl_3$ [29]. In fact, for all of the systems, the experimental data were not sufficient to vary all the free-ion parameters at a time during fitting. Four of the atomic parameters (M^2, M^4, P^4 and P^6) were constrained according to $M^2 = 0.56M^0$, $M^4 = 0.38M^0$, $P^4 = 0.75P^2$ and $P^6 = 0.50P^2$. The values of $\alpha = 22.12$, $\beta = -656$, $\gamma = 1583$, $T^2 = 372$, $T^3 = 40$, $T^4 = 61$, $T^6 = -291$, $T^7 = 347$, $T^8 = 355$, $M^0 = 1.84$ and $P^2 = 281$ are fixed in the parameterization. The best-fit free-ion parameter values are shown in table 3, and using these parameters, the calculated energy levels are obtained by diagonalizing the energy matrix of $4f^3$ (Nd^{3+}) configuration. However, the fits may be improved by allowing all the free-ion parameters to vary, but in the present analysis only a few of the most important parameters are varied and all the remaining ones are fixed to have better qualitative comparison.

The nephelauxetic ratio, β, and the bonding parameter, δ, are calculated using equation (3), using the free-ion energy levels reported by Carnall *et al* [23]. The negative quantities of bonding parameters δ for all the systems indicate that the bonding of Nd^{3+} ions with the local host is ionic. Based on the relative magnitude of δ (cm^{-1}) values, among the various glasses, it is found that PKBAFN(2) exhibits higher ionic character ($\delta = -19.355$) whereas PKBFAN(2) exhibits lower ionic character ($\delta = -18.567$). The net electrostatic effects ($\sum_k F^k$, cm^{-1}) experienced by the Nd^{3+} ion in the title 1.0 mol% glasses varied in the order of PKBAFN(2) (161 480) < PKBFAN(2) (161 663) < PKBAN(2) (162 461) and are found to be relatively greater than that for free-ion (129 014). As seen from the trends of hydrogenic ratios within the title glasses, there is no systematic variation since F^2/F^4 was found to be maximum for PKBAN(2) whereas F^2/F^6 was found to be maximum for PKBFAN(2). However, F^2/F^4 and F^2/F^6 for the title glasses are relatively lower than those found for the free ion. This trend suggests that a considerable amount of expansion of $4f^3$ configuration is noticed in title glasses. The free-ion parameters and the hydrogenic ratios derived for Nd:PSP glass differ considerably; this may be due to the lower number of levels used for energy level analysis as noticed in the earlier energy level analysis [6, 29].

5.3. Oscillator strengths and Judd–Ofelt analysis

The Judd–Ofelt theory provides a reasonably good description for the spectral transition intensities of Nd^{3+} ions in the glass matrices. As seen from table 4, the experimental oscillator strengths observed in the present glasses are in close agreement with the calculated ones with root-mean-square deviation values ± 0.59 (PKBAN(2)) and ± 0.68 (PKBFAN(2)) and ± 0.64 (PKBAFN(2)). From table 4, it is obvious that the non-symmetric component of the electric field acting on Nd^{3+} ions is relatively higher in glasses under investigation than those in FBP and BKP glasses since most of levels in the present case possess relatively higher oscillator strengths.

Table 5 presents the JO parameters (Ω_λ, $\lambda = 2$, 4 and 6) for the neodymium-doped glasses. Among the glasses under investigation, based on the order of the Ω_2 value, it is evident that the disorder increased in the sequence PKBFAN(2) < PKBAFN(2) < PKBAN(2). Also it is obvious that there is no uniform trend of variations in JO parameters since the observed trend is $\Omega_4 < \Omega_6 < \Omega_2$ for PKBAN(2), $\Omega_2 < \Omega_6 < \Omega_4$ for PKBFAN(2) and $\Omega_4 < \Omega_2 < \Omega_6$ for PKBAFN(2). Further, the value of Ω_6 is observed to decrease in the sequence PKBAN(2) > PKBFAN(2) > PKBAFN(2), indicating that Nd^{3+} ions experience stronger rigidity in PKBAFN(2) glass.

The spectroscopic quality parameter (X) and the quantum efficiency (η) are also presented in table 5. The X and η values were found to be relatively higher for PKBFAN(2) glass than for those glasses listed in table 5. Interestingly the X values found for PKBAFN(2) are quite similar to that for commercial glass [1, 28]. The derived η for title glasses are relatively higher than those found for FBP and BKP glasses.

5.4. Emission spectra

The emission spectra for the glasses under investigation are shown in figure 2. The emission band wavelength, experimental and calculated branching ratios, the peak stimulated emission cross sections and effective bandwidths are reported in table 6. From this table, it is obvious that there is no significant effect of chemical composition on the emission band wavelength (λ_p) for all the systems. It is noticed that the present glasses possess relatively higher cross-sections than those previously reported [1, 2, 24, 28].

The values of branching ratios (β_R) for the $^4F_{3/2} \rightarrow {}^4I_J$ ($J = 15/2, 13/2, 11/2$ and $9/2$) transition depend on the Ω_4/Ω_6 since Ω_2 does not contribute in determining the intensity of these bands as $\|U^2\|^2$ is zero for these transitions. This relation allows us to compare the branching ratios versus JO intensity parameter ratios. In general, Ω_4/Ω_6 is nearly unity for most of the commonly reported phosphate laser compositions. To be more specific, in the metaphosphate laser glass compositions, approximately 40% of transitions terminate at the $^4I_{9/2}$ state, 50% at the $^4I_{11/2}$ state, 10% at the $^4I_{13/2}$ state and typically less than 0.5% radiates to the $^4I_{15/2}$ state [1], which is similar to our derived values (table 6). The experimental and calculated β_R for Nd^{3+}-doped borate crystals [30] exhibit a similar trend and also those values are comparable with the present glasses.

5.5. Luminescence decay and non-radiative processes

When the Nd^{3+} ion is excited from its ground state to the levels having energy higher than that of $^4F_{3/2}$, they decay non-radiatively to lower levels down to the $^4F_{3/2}$ state due to very small energy gaps between the adjacent energy levels. As the energy gap between the metastable $^4F_{3/2}$ level and its lower level $^4I_{15/2}$ is sufficiently large (5600 cm^{-1} approximately), radiative transitions will predominate here over the non-radiative transitions (figure 4).

The radiative lifetime of the $^4F_{3/2}$ state depends upon the values of JO parameters, especially on Ω_4 and Ω_6, as well as on the host refractive index. It represents a mean value over the different sites occupied by the Nd^{3+} ions in the glass matrix and it is higher than that determined experimentally from the luminescence decay. This reduction in experimental lifetime can be explained by considering all the possible relaxation processes relative to the excited Nd^{3+} ions.

If the experimentally measured lifetime of the emitting state is denoted by τ, then the total decay rate ($1/\tau$) is the sum of radiative (A_r) and non-radiative (W_{n-r}) decay rates. Therefore,

$$1/\tau = A_r + W_{n-r}. \tag{16}$$

In phosphate glasses, principally, there are four non-radiative processes contributing to the reduction of measured lifetime of the emitting level.

$$W_{n-r} = W_{m-p} + W_{c-q} + W_{e-t} + W_{OH} \tag{17}$$

where W_{m-p}, W_{c-q}, W_{e-t} and W_{OH} denotes the non-radiative decay rates corresponding to the multiphonon relaxation process, concentration quenching, energy transfer to another doping impurity and hydroxyl (OH^-) groups, respectively. W_{m-p} decreases exponentially as the

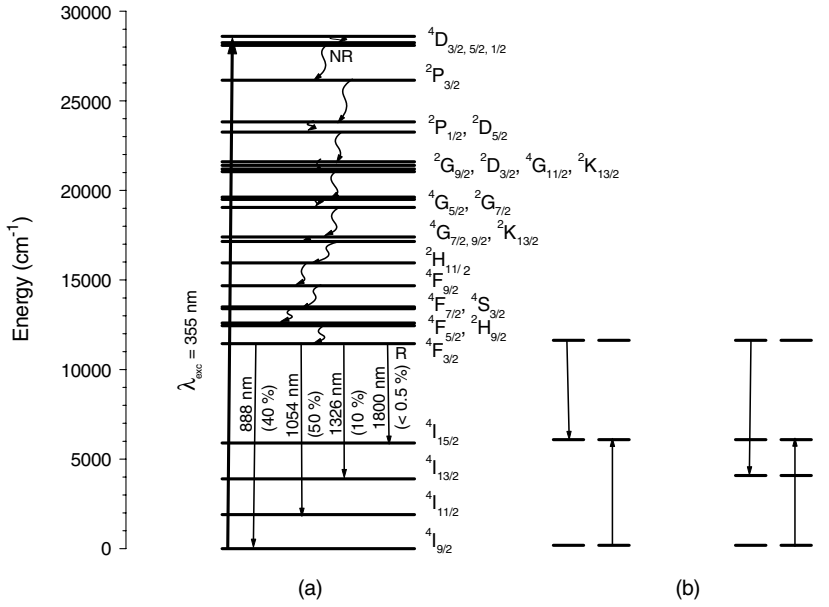

Figure 4. Energy level diagram of Nd^{3+} ion with (a) radiative (R, shown by straight arrows) and non-radiative (NR, shown by curved arrows) transitions and (b) cross-relaxation channels.

energy gap between the neighboring energy levels increases [31, 32]. For the Nd^{3+} ion, the energy gap between the $^4F_{3/2}$ level and its lower level $^4I_{15/2}$ is sufficiently large enough that W_{m-p} is negligible compared to the radiative decay rate of the $^4F_{3/2}$ level of the Nd^{3+} ion in phosphate glasses [33, 34].

For weak concentrations, the non-radiative relaxations due to ion–ion interactions (W_{c-q} and W_{e-t}) will be almost negligible and the radiative lifetime will be in agreement with that of experimental values. But our systems have shown a slightly non-exponential shape of the decay curves even at low concentrations ($<0.25 \times 10^{20}$ ions cm^{-3}) indicating that there is a slight chance for a non-radiative process, most probably by cross-relaxation and the transfer of energy to OH^- ions. It is also reported that enhanced lifetimes have been noticed in Nd:YAG nanostructures on removing OH^- radicals from the closest surroundings of Nd^{3+} ions [35].

In all the glass systems PKBAN, PKBFAN and PKBAFN as already discussed above, the lifetime is decreased with increase in concentration of acceptors (Nd^{3+} ions). The decay curves for all three concentrations in all the glasses are found to be non-exponential and this non-exponential nature increases with increase of Nd^{3+} ion concentration due to enhanced energy transfer by cross-relaxation between two Nd^{3+} ions [2]. This is also clearly evident from the decreased lifetimes of the $^4F_{3/2}$ level in PKBAN (decreased from 232 to 121 μs), PKBFAN (decreased from 256 to 132 μs) and PKBAFN (decreased from 234 to 131 μs) glasses when the concentration of Nd^{3+} ions is increased from 0.1 to 2.0 mol%.

The non-exponential nature of the decay curves is well fitted to the Inokuti–Hirayama model for $S = 6$, indicating that the dominant interaction for energy transfer through cross-relaxation between Nd^{3+} ions is of dipole–dipole type. The channels that could be responsible for cross-relaxation of Nd^{3+} ions are $(^4F_{3/2} + {}^4I_{9/2}) \rightarrow (^4I_{15/2} + {}^4I_{15/2})$ or $(^4F_{3/2} + {}^4I_{9/2}) \rightarrow (^4I_{13/2} + {}^4I_{15/2})$ [31, 33] (see figure 4). Similar results of concentration quenching of the emission of Nd^{3+}-doped materials have also been reported [36–38]. The derived parameters from IH fits are presented in table 7. The energy-transfer fitting parameter

Q is increased whereas the donor–acceptor separation (R_0) and dipole–dipole interaction parameter (C_{DA}) are decreased with increase in concentration. From table 7, it is noticed that the value of R_0 is less than the average distance, $R(R = (3/4\pi N_0)^{1/3})$, between the donor and acceptor. It is also obvious that the values of Q, C_{DA} and W_{n-r} are found to decrease when the glasses are modified with fluoride compounds. The values of τ_0, R_0 and C_{DA} obtained for the present glasses are found to be relatively higher than those values derived for Nd:YAG [36] and Nd^{3+}:$YAlO_3$ [37].

6. Conclusions

The spectroscopic properties of Nd^{3+}-doped phosphate and fluorophosphate glasses for three concentrations of Nd^{3+} ions are studied and are found to be comparable with the reported values. Radiative properties are predicted for 1.0 mol% doped glasses using the best-fit JO parameters derived from their respective absorption spectra and are comparable with the experimental values. The relatively higher Ω_2 value for the present systems represent a stronger covalent bond and a lower symmetry for their structure compared to other reported glass systems. This is clearly supported by the relatively larger emitting wavelengths compared to the reported commercial system. The measured decay curves for all the three concentrations of Nd^{3+} ions in the title glasses are found to be non-exponential. Increase of non-exponential nature and decrease of lifetime of the $^4F_{3/2}$ level are noted when the concentration of Nd^{3+} is increased from 0.1 to 2.0 mol% in all the glass systems. The IH model analysis on the non-exponential nature of the decay curves reveals that the interaction responsible for cross-relaxation between the acceptor and donor ions is of dipole–dipole type. These studies are helpful for optimizing the glass composition to enhance the laser properties of Nd^{3+}:phosphate glasses.

Acknowledgments

This work has been carried out under the financial assistance of a major research project provided by DAE-BRNS, Government of India (Sanction No. 2003/34/4-BRNS/600, dt. 11.07.2003) and MIUR of Italy.

References

[1] Campbell J H and Suratwala T I 2000 *J. Non-Cryst. Solids* **263/264** 318
[2] Ajroud M, Haouari M, Ben Ouada H, Maaref H, Brenier A and Garapon C 2000 *J. Phys.: Condens. Matter* **12** 3181
[3] Snitzer E 1961 *Phys. Rev. Lett.* **7** 444
[4] Hufner S 1978 *Optical Spectra of Transparent Rare Earth Compounds* (New York: Academic)
[5] Renuka Devi A and Jayasankar C K 1995 *Mater. Chem. Phys.* **42** 106
[6] Rukmini E and Jayasankar C K 1995 *Physica* B **212** 167
[7] Jayasankar C K and Ravi Kanth Kumar V V 1996 *Physica* B **226** 313
[8] Yin M, Li Y, Dong N, Makhov V N, Khaidukov N M and Krupa J C 2003 *J. Alloys Compounds* **353** 95
[9] Sinha S P 1966 *Complexes of the Rare Earths* (Oxford: Pergamon)
[10] Weber M J, Myers J D and Blackburn D H 1981 *J. Appl. Phys.* **52** 2944
[11] Weber M J, Ziegler D C and Angell C A 1982 *J. Appl. Phys.* **53** 4344
[12] Gatterer K, Pucker G, Jantscher W, Fritzer H P and Arafa S 1998 *J. Non-Cryst. Solids* **231** 189
[13] Speghini A, Peruffo M, Casarin M, Ajo D and Bettinelli M 2000 *J. Alloys Compounds* **300/301** 174
[14] Dewar A L, Mehta V, Mansingh A and Rup R 1997 *Opt. Mater.* **7** 33
[15] Carnall W T, Gschneidner K A and Eyring L (ed) 1987 *Hand Book on the Physics and Chemistry of Rare Earths* vol 3 (Amsterdam: North-Holland) chapter 24
[16] Judd B R 1962 *Phys. Rev.* **127** 750

[17] Ofelt G S 1962 *J. Chem. Phys.* **37** 511
[18] Brown D C 1981 *High-Peak Power Nd:Glass Laser Systems* (*Springer Series in Optical Sciences*) (Berlin: Springer)
[19] Fujii S T, Kodaira K, Kawauchi O, Tanaka N, Yamashita H and Anpo M 1997 *J. Phys. Chem.* B **101** 10631
[20] Inokuti M and Hirayama F 1965 *J. Chem. Phys.* **43** 1978
[21] Antic-Fidancev E, Lemaitre-Blaise M, Beaury L, Teste de Sagey G and Caro P 1980 *J. Chem. Phys.* **73** 4613
[22] Lakshman S V J and Suresh Kumar A 1988 *J. Phys. Chem. Solids* **49** 133
[23] Carnall W T, Goodman G L, Rajnak K and Rana R S 1988 *Argonne National Laboratory Report* ANL-88-8, IL
[24] Kumar G A, De la Rosa-Cruz E, Martinez A, Unnikrishnan N V and Ueda K 2003 *J. Phys. Chem. Solids* **64** 69
[25] Binnemans K, Van Deun R, Gorller-Warland C and Adam J L 1998 *J. Alloys Compounds* **275–277** 455
[26] De la Rosa-Cruz E, Kumar G A, Diaz-Torres L A, Martinez A and Barbosa-Garcia O 2001 *Opt. Mater.* **18** 321
[27] Mehta V, Aka G, Dewar A L and Mansingh A 1999 *Opt. Mater.* **12** 53
[28] *Laser Glass Product Catalog* 1999 (Duryea, PA: Schott Technologies) p 1
[29] Rukmini E, Jayasankar C K and Reid M F 1994 *J. Phys.: Condens. Matter* **6** 5919
[30] Chen X, Luo Z, Jaque D, Romero J J, Garcia Sole J, Huang Y, Jiang A and Tu C 2001 *J. Phys.: Condens. Matter* **13** 1171
[31] Ebendorff-Heidepriem H, Seeber W and Ehrt D 1995 *J. Non-Cryst. Solids* **183** 191
[32] Layne C B, Lowdermilk W H and Weber M J 1977 *Phys. Rev.* B **16** 10
[33] Liegard E, Doualan J L, Moncorge R and Bettinelli M 2005 *Appl. Phys.* B **80** 985
[34] Caird J A, Ramponi A J and Staver P R 1991 *J. Opt. Soc. Am.* **B8** 1391
[35] Hreniak D, Strek W and Mazur P 2002 *Mater. Sci.* **20** 40
[36] Lupei V, Lupei A, Georgescu S and Yen W M 1989 *J. Appl. Phys.* **66** 3792
[37] Lupei V, Lupei A and Georgescu S 1992 *J. Phys.: Condens. Matter* **4** L221
[38] Ehrmann P R and Campbell J H 2002 *J. Am. Ceram. Soc.* **85** 69